Title of paper: **Particle breakage during cyclic triaxial loading of a carbonate sand**

Names of authors: Dr. Shane Donohue[1], Dr. Catherine O'Sullivan[2], Dr. Michael Long[1]

Affiliation of authors: 1 School of Architecture, Landscape and Civil Engineering, University College Dublin (UCD)

2 Dept. of Civil and Environmental Engineering, Imperial College London

Contact address: Shane Donohue, School of Architecture, Landscape and Civil Engineering, University College Dublin (UCD), Newstead building, Belfield, Dublin 4, Ireland.

Phone: +353-87-9711917

Fax: +353-1-7163297

e-mail: shane.donohue@ucd.ie

Keywords: calcareous soils, laboratory tests, sands

INTRODUCTION

Dynamic loading of embankment, foundation and pavement structures results in particle breakage of the constituent granular materials, when the stresses imposed on their particles exceed their strength. Particle breakage is dependent on a number of "macro-scale" parameters (e.g. stress level, grading, void ratio) as well as on the characteristics (e.g. size, shape, strength, mineral composition) of the constituent particles (Hardin 1985; Coop 1990; Lade et al. 1996; McDowell & Bolton 1998; Nakata et al. 2001; Coop et al. 2004; Leleu & Valdes 2007). A number of recent detailed studies have considered the relationship between particle crushing and soil response. For example, Coop et al (2004) demonstrated a link between particle breakage and volumetric compression, and showed using a series of ring shear tests that particle crushing during shearing continues to very large strains. Cheng et al (2003) used DEM (discrete element modelling) to demonstrate a link between particle crushing and response along the normal compression line, while Lackenby at al. (2007) studied the effect of confining pressure on ballast degradation under cyclic triaxial loading. Particle breakage is generally quantified through a comparison of pre and post crushing particle size distribution curves (Hardin 1985).

Photoelasticity studies (e.g. Drescher & De Josselin de Jong, 1972) and DEM simulations (e.g. Cundall & Strack 1979) have both demonstrated that the distribution of stress in a granular material is highly heterogeneous. Particles do not equally share in the bearing of load, and those with highly loaded contacts are usually aligned in chains or columns. O'Neill (2005) simulated a series of strain controlled cyclic biaxial tests on a 2D granular material using PFC2D (Itasca, 2002), some of the results of which are presented in Figure 1. The specimen configuration considered by O'Neill, included 7771 circular (disk) shaped particles with diameters varying between 2 and 3 mm (Figure 1a). Following isotropic compression a series of strain controlled load cycles were applied to the specimen. In each cycle the axial compressive strain was increased to ε_a = 1% and then

reduced to ε_a = 0%. The distribution of interparticle forces though the specimen at ε_a = 1% is shown for the first and fourth load cycles in Figures 1(b) and 1(c) respectively. To illustrate both the magnitude and orientation of the interparticle contact forces in the DEM simulations, a line is drawn between the centroids of contacting particles, the thickness of which is weighted to be proportional to the magnitude of the compressive force between these particles. This approach is often used to visualise force chains in granular materials (e.g. Thorton and Barnes (1986)). As shown the force network is not the same in both cases, i.e. different particles are experiencing the largest forces from cycle to cycle. We can reasonably anticipate that degradation in the form of breakdown of asperities and particle crushing is associated with particles participating in the strongest force chains (McDowell et al. 1996; Cheng et al. 2001; Vallejo et al. 2006). If these force chains are not static as shown by O'Neill (2005), then additional damage to the material should occur in each cycle.

The objective of the current study is to consider a realistic granular material known to exhibit crushing and explore the degradation of this material during drained cyclic triaxial loading by quantifying particle breakage. The study considers the sensitivity of the response both to the mean effective stress (p') value and the number of cycles of loading.

MATERIALS AND METHODS

Loose carbonate sands of biogenic origin tend to crush more easily than silica based sands, as their fragile shell particles fracture (Coop, 1990). The crushing of these materials may occur even at relatively low pressures (Coop & Lee, 1993), thereby facilitating research into particle crushing. In the current study the biogenic carbonate sand considered was obtained from Dogs Bay on the west coast of Ireland. Dogs Bay sand consists of angular mollusc, gastropod and forminifera fragments (Golightly, 1989). As a result of the open

structure created by these angular particles, the sand has a high initial void ratio. The material is poorly graded (Figure 2), with a carbonate content of 88-94% (Houlsby et al. 1988). The engineering behaviour and properties of the material have been examined in detail by a number of researchers (e.g. Houlsby *et al.* 1988; Golightly 1989; Coop 1990; Coop & Lee 1993; Yasufuku & Hyde 1995; Hyodo *et al.* 1998; Coop et al. 2004; Tarantino & Hyde 2005; Qadimi & Coop 2007). There is some variability among the particle size distributions (Figure 1) and index properties (Table 1) reported in the literature. These variations are likely due to different sampling locations at Dog's Bay. For example Golightly (1989) and Coop et al. (1993) used sand from the dunes, whereas Tarantino & Hyde (2005) used material from the intertidal zone. In the current study the sand was sampled from the intertidal zone.

It has been shown that particle breakage is greater for uniformly graded than for well graded sands (Nakata et al., 2001; Coop et al. 2004). Therefore in order to maximise breakage potential tests were performed on material from the 300–425μm sieve interval. This sieve interval was also used by Coop et al. (2004) in their ring shear tests. Due to the highly crushable nature of the material, wet sieving was necessary to ensure that additional damage did not occur during preparation. As shown in Table 1, e_{max} is considerably higher for this uniform grading than the natural grading. Samples of 50mm diameter were prepared by pluviation into a water-filled membrane, held within a mould on the triaxial pedestal. This approach was used to provide very loose samples which were both consistent and comparable. The soil, which was first submerged under water and placed under a vacuum, to assist saturation, was transferred to the membrane in a spoon (also under water). The triaxial tests were conducted using a GDS computer-controlled Bishop & Wesley system, which had a maximum cell pressure of 1700kPa.

After saturation to an acceptable level (i.e. a Skempton B value of at least 0.95) a stage of isotropic compression was applied at a rate of 25kPa per hour up to the desired pressure (mean effective stress, p' of either 100kPa, 500kPa or 1000kPa). The low rate of compression minimised creep (Qadimi & Coop 2007) thereby reducing the resting period prior to cycling. McDowell & Khan (2003) have shown that creep of granular materials is accompanied by particle crushing, therefore in order to control creep, the final isotropic compression pressures were maintained until the rate of increase of volumetric strain was less than 0.003% per hour. Details of the tests conducted are provided in Table 2, including the volumetric strain measured during isotropic compression. Although every effort was made to ensure that each sample tested was as similar / loose as possible, there was a small degree of variability in the initial void ratios (e_0) for the tests.

Each of the cyclic tests were drained, and all of the tests were designed to have cycles of loading symmetrical about the isotropic axis with a cyclic stress ratio β^* (= $\Delta q_{max}/p'_i$), usually of 20%. This value was selected as it resulted in reasonably significant changes in volumetric strain within a relatively short number of cycles, without the generation of excess pore pressures. One of the tests isotropically compressed to a p' of 500kPa was subjected to a β^* of 10%. Sinusoidal cycles with a period of 120s were applied to all cyclic tests using the GDS system. This was within the range used by Qadimi & Coop (2007), who observed a negligible effect on the pore pressure response of drained cyclic tests with periods ranging between 90–1800s.

At each of the three effective stress levels under investigation tests were performed with 150 and 1000 cycles (Table 2). A 5000 cycle test was also performed at the p'=500kPa stress level (test Dogs 10). A number of specimens were also simply compressed isotropically to the desired stress level (zero cycles). Following testing, the final sample dimensions and mass were measured, and the final particle size distribution

was determined. The amount of particle breakage was quantified by the relative breakage (B_r) parameter of Hardin (1985). For this study material retained in the British Standard 0.063mm sieve was taken as the minimum particle size below which breakage was deemed insignificant. Although Hardin (1985) used a US Standard 0.074mm sieve in his definition of relative breakage the effect on the calculated values was found to be negligible.

RESULTS

Volume change during cycling

The volumetric strain behaviour of the tests undergoing cyclic loading are shown in Figure 3(a, b and c) for tests undergoing 150, 1000 and 5000 cycles respectively. As shown in Figures 3(a) and 3(b) cyclic tests at a p' of 1000kPa experienced more than twice the volumetric strain of those tests at 500kPa. Considering the 150 cycle tests, significantly less volumetric strain was observed when using a β^* of 10%. Where 1000 cycles of loading were applied (Figure 3(b)), it is apparent that a significant portion (approx. 60 - 70%) of the cyclic-induced volumetric strain develops over the initial 100-150 cycles. The volumetric strain increases at an approximately constant rate after the initial 150 - 250 cycles until the end of the test, certainly indicating a continued change to the specimen fabric and possibly implying continued particle crushing. A cessation of volumetric strain was not observed, even after 5000 cycles (Figure 3(c)).

A single test (Dogs 8) was carried out to examine the effect of creep on the observed response. In this test the cyclic loading stage was conducted shortly after the end of isotropic compression, thereby limiting creep. The results presented in Figure 3(b) illustrate that this sample experienced greater volumetric strain during cyclic loading than Dogs 9, which was allowed to creep. This was also observed by Qadimi & Coop (2007),

who noted an increase in the pore pressure response of undrained cyclic tests that were given insufficient time to creep.

Quantification of Particle Breakage

The particle size distribution tests at each stress level are presented in Figure 4. Although the majority of volumetric strain clearly occurs during isotropic compression (Table 2), there is a clear reduction in particle size with increasing number of cycles at each stress level (particularly at p'=500kPa and 1000kPa). As shown in Figure 4(b), the particle size distribution of the 5000 cycle test is very similar to the 1000 cycle test, containing only a slightly greater amount of finer particles, indicating minimal additional breakage. As expected the 150 cycle test with β^*=20% generates finer particles than the test using a β^*=10%. The relationship between Hardin's relative breakage (B_r) and number of cycles from tests with 1000 cycles or less is illustrated in Figure 5. The relationship is similar to that shown in Figure 3 for volumetric strain, with significantly more breakage occurring in the first 150 cycles (approx. 55 - 70%), in comparison with the subsequent 850 cycles. Increasing the number of cycles generally resulted in a corresponding increase in particle breakage, although at the 100kPa stress level the differences in B_r were very small.

The relationship between Hardin's relative breakage (B_r) and total volumetric strain (isotropic plus cyclic) from all tests is illustrated in Figure 6(a). As shown a clear relationship exists between these two parameters. Coop et al. (2004) also observed a strong correlation between these parameters. It is again clear that breakage is strongly influenced by the number of cycles. The amount of breakage occurring directly as a result of drained cycling (not including isotropic compression) is examined in Figure 6b. On this occasion the particle size of the zero cycle tests (isotropically compressed only) are taken

as the minimum, and the amount of breakage directly due to cycling is calculated relative to this grading for all tests. Despite the small differences in B_r, a strong relationship clearly exists between this parameter and volumetric strain due to cycling.

The breakage data from this study is compared to that of Coop & Lee (1993) in Figure 7, who measured particle breakage after a series of monotonic loading tests on specimens of naturally graded Dogs Bay sand. As illustrated in this figure, the measurements of particle breakage from the current study compare well with their isotropically compressed tests, despite the uniform grading used here. As discussed above, increasing the number of cycles results in greater particle breakage, and therefore at a given p' the B_r values observed plot further from the NCL, as estimated by Coop & Lee (1993).

CONCLUSIONS

This paper has presented the results of a number of drained cyclic triaxial tests on loose, uniformly graded samples of carbonate sand, which were firstly isotropically compressed to a specified stress level. It was observed that particle breakage is dependent on stress level, cyclic stress ratio, and creep and is directly related to volumetric strain. Drained cycling increases volumetric strain and therefore more breakage occurs when larger numbers of cycles are imposed. A large portion of the total volumetric strain/particle breakage occurred initially, after which a constant rate of increase was observed. Particle breakage was also measured at low stress levels (p' = 100kPa) although in small quantities.

The findings of this research can be qualitatively related to the earlier DEM simulations of O'Neill (2005). In the current study, the increase in particle breakage from one cycle to the next indicates that while particles may not be loaded to their full capacity in a given cycle, they can be crushed in subsequent cycles without any variation in the

amplitude of cyclic loading. The micromechanical explanation (informed by O'Neill's work) is that the contact force network evolves from one cycle to the next, with different particles participating in the most highly loaded branches of the contact force network from cycle to cycle. Hence new particles will experience load sufficient to crush them in each cycle. This response does not however continue indefinitely and it may be that the material reaches a "stable" grading after a sufficient number of cycles. However, further micro-mechanics studies are needed before a definite theory can be proposed to explain the mechanics underlying the observed decrease in the rate of volumetric strain and particle crushing as cyclic loading progresses.

ACKNOWLEDGEMENTS

Funding for this research was provided by the Irish Research Council for Science, Engineering and Technology (ISCSET) under the Basic Research Grant Scheme. The authors also would like to thank Pierse construction for their assistance.

NOTATION

B	pore water pressure coefficient
B_r	relative breakage, Hardin (1985)
D_{50}	mean particle size
G_s	specific gravity
e_0	initial void ratio
e_{min}	minimum void ratio
e_{max}	maximum void ratio
p'	mean normal effective stress [= $(\sigma'_a + 2\sigma'_r) / 3$]
p'_i	initial p' at the start of cyclic loading
q	deviatoric stress (= $\sigma'_a - \sigma'_r$)

β^* cyclic stress ratio (= $\Delta q_{max} / p'_i$)

ε_a axial strain

ε_v volumetric strain

REFERENCES

Cheng, Y. P., White, D. J., Bowman, E. T., Bolton, M. D. & Soga, K. (2001). The observation of soil microstructure under load. *Proc. Powders and Grains 2001*, Sendai, 69–72.

Cheng, Y. P., Nakata, Y. & Bolton, M. D. (2003). Discrete element simulation of crushable soil. *Géotechnique* **53**, No. 7, 633–641.

Coop, M.R. (1990). The mechanics of uncemented carbonate sands. *Géotechnique* **40**, No. 4, 607-626.

Coop, M. R. & Lee, I. K. (1993). The behaviour of granular soils at high stresses. In *Predictive Soil Mechanics: Proceedings of the Wroth Memorial Symposium on predictive soil mechanics*, pp. 186–198. London: Thomas Telford.

Coop, M. R., Sorensen, K. K., Bodas Freitas, T. & Georgoutos, G. (2004). Particle breakage during shearing of a carbonate sand. *Géotechnique* **54**, No. 3, 157–163.

Cundall, P. A., & Strack, O. D. L. (1979). A discrete numerical model for granular assemblies. *Géotechnique* **29**, No. 1, 47–65.

Drescher, A., De Josselin de Jong, G. (1972). Photoelastic verification of mechanical. model for the flow of a granular material. *J. Mech. Phys. Solids* **20**, No. 5, 337-351

Golightly, C. R. (1989). Engineering properties of carbonate sands. *PhD thesis*, University of Bradford, UK.

Hardin, B.O. (1985). Crushing of soil particles. *J. Geotech. Engng., ASCE* **111**, No. 10, 1177-1192.

Houlsby, G.T., Evans, K.M. & Sweeney, M. (1988). End bearing capacity of model piles in layered carbonate soils. *Proc. Int. Conf. on Calcareous Sediments,* Perth, Australia, **1**, 209-214.

Hyodo, M., Hyde, A.F.L. & Aramaki, N. (1998). Liquefaction of crushable soils. *Géotechnique* **48**, No. 4, 527-543.

Itasca Consulting Group (2002). PFC2D – Particle Flow Code in Two Dimensions. Version 3·00. Minneapolis: ICG.

Klotz, E.U. (2000). Influence of state on the capacity of driven piles in sand. *PhD thesis*, City University, London, UK.

Lackenby, J., Indraratna, B., McDowell, G. and Christie, D. (2007). Effect of confining pressure on ballast degradation and deformation under cyclic triaxial loading. *Géotechnique* **57**, No. 6, 527-536.

Lade, P. V., Yamamuro, J. A. & Bopp, P. A. (1996). Significance of particle crushing in granular materials. *J. Geotech. Engng., ASCE* **122**, No. 4, 309–316.

Leleu, S. L. & Valdes, J. R. (2007). Experimental study of the influence of mineral composition on sand crushing. *Géotechnique* **57**, No. 3, 313–317.

McDowell, G. R., Bolton, M. D. & Robertson, D. (1996). The fractal crushing of granular materials. *J. Mech. Phys. Solids* **44**, No. 12, 2079–2102.

McDowell, G. R. & Bolton, M. D. (1998). On the micromechanics of crushable aggregates. *Géotechnique* **48**, No. 5, 667–679.

McDowell, G. R. & Khan, J. J. (2003). Creep of granular materials. *Granular Matter* **5**, No. 3, 115–120.

Nakata, Y., Hyodo, M., Hyde, A. F. L., Kato, Y. & Murata, H. (2001). Microscopic particle crushing of sand subjected to high pressure one dimensional compression. *Soils and Foundations* **41**, No. 1, 69–82.

O'Neill, S. (2005). A fundamental examination of the beheviour of granular media and its application to discrete element modelling, *MEng.Sc thesis*, University College Dublin, Ireland.

Qadimi, A. and Coop, M.R. (2007). The undrained cyclic behaviour of a carbonate sand. *Géotechnique* **57**, No. 9, 739–750.

Tarantino, A. and Hyde, A.F.L. (2005). An experimental investigation of work dissipation in crushable materials *Géotechnique* **55**, No. 8, 575-584.

Thornton, C. and Barnes, D.J. (1986). Computer simulated deformation of compact granular assemblies. *Acta Mechanica* **64** 1, pp. 45–61.

Vallejo, L.E., Lobo-Guerrero, S., and Hammer, K. (2006). Degradation of a Granular Base under a Flexible Pavement: DEM Simulation. *International Journal of Geomechanics* **6**, No. 6, 435–439.

White, D.J. (2002). An investigation into the behaviour of pressed in piles. *PhD thesis*, University of Cambridge, UK.

Yasufuku, N. & Hyde, A. F. L. (1995). Pile end-bearing capacity in crushable sands. *Géotechnique* **45**, No. 4, 663-676.

FIGURE CAPTIONS

Figure 1 Illustration of dynamic distribution of force chains in cyclic 2D DEM simulations (a) Initial specimen configuration (b) Distribution of strong force chains at axial strain of 1% - cycle 1 (c) Distribution of strong force chains at axial strain of 1% - cycle 4

Figure 2 Particle size distribution, comparison of current study with earlier research on Dog's Bay Sand

Figure 3 Volumetric strain behaviour during cyclic loading for tests subjected to (a) 150 cycles (b) 1000 cycles (c) 5000 cycles.

Figure 4 Evolution of particle size distribution for tests at a mean effective stress (p') of (a) 100kPa (b) 500kPa (c) 1000kPa.

Figure 5 The variation of Hardin's relative breakage with number of cycles.

Figure 6 (a) The variation of Hardin's relative breakage with total volumetric strain (isotropic + cycling) (b) The variation of Hardin's relative breakage (cyclic only) with volumetric strain produced during cycling.

Figure 7 Comparison between particle breakage measured after monotonic loading tests by Coop & Lee, (1993), and tests from this study.

Reference	**G_s**	**D_{50} (mm)**	**e_{max}**	**e_{min}**
Golightly (1989), White (2002)	2.75	0.44	1.87	0.98
Yasufuku & Hyde (1995), Hyodo et al. (1998)	2.72	0.22	2.45	1.62
Klotz (2000)	2.71	0.20	1.84	1.37
This Study	2.70	0.33	1.86	1.17
This Study (300-425 sieve interval)	2.70	-	2.22	1.14

Table 1. Dogs Bay index properties as reported in the literature and in this study.

Test number	**e_0**	**p'** **(kPa)**	**$\varepsilon_{v\ iso}$ (isotropic compression only)** **(%)**	**Number of cycles**	**$\varepsilon_{v\ cyc}$ (cyclic)** **(%)**
Dogs 1	2.01	100	1.11	0	
Dogs 2	2.06	100	1.25	150	0.14
Dogs 3	1.96	100	1.33	1000	0.07
Dogs 4	1.85	100	1.06	1000	0.15
Dogs 5	1.87	500	4.05	0	
Dogs 6	1.95	500	4.59	150	0.62
Dogs 7 (β=10%)	1.97	500	4.52	150	0.20
Dogs 8	1.97	500	4.14	1000	1.27
Dogs 9	1.90	500	4.16	1000	1.03
Dogs 10	1.96	500	4.01	5000	1.75
Dogs 11	1.92	1000	12.20	0	
Dogs 12	1.97	1000	12.46	150	2.12
Dogs 13	1.85	1000	12.09	1000	2.93

Table 2. Summary of the test data

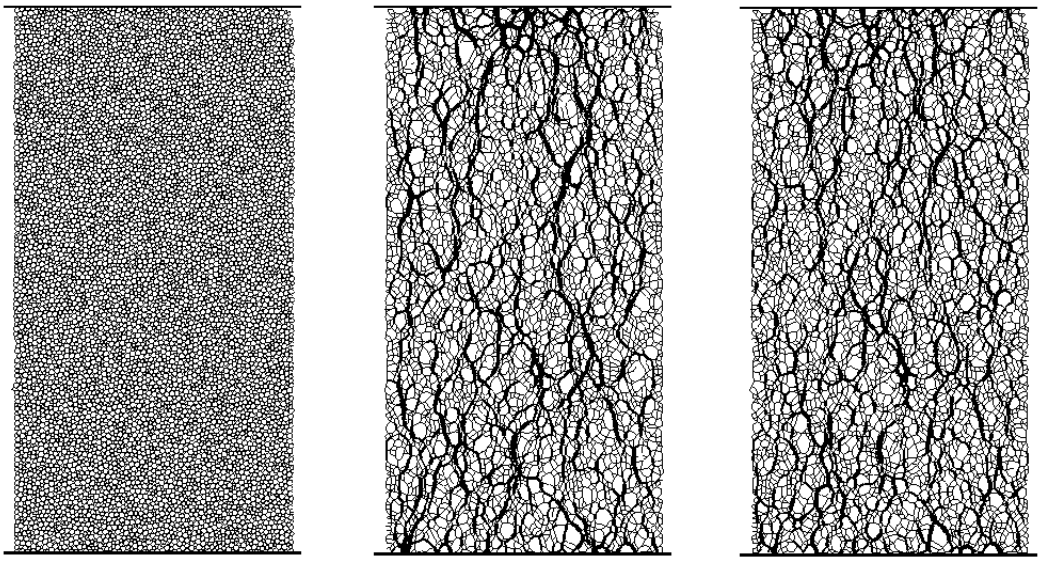

Figure 1 Illustration of dynamic distribution of force chains in cyclic 2D DEM simulations (a) Initial specimen configuration (b) Distribution of strong force chains at axial strain of 1% - cycle 1 (c) Distribution of strong force chains at axial strain of 1% - cycle 4

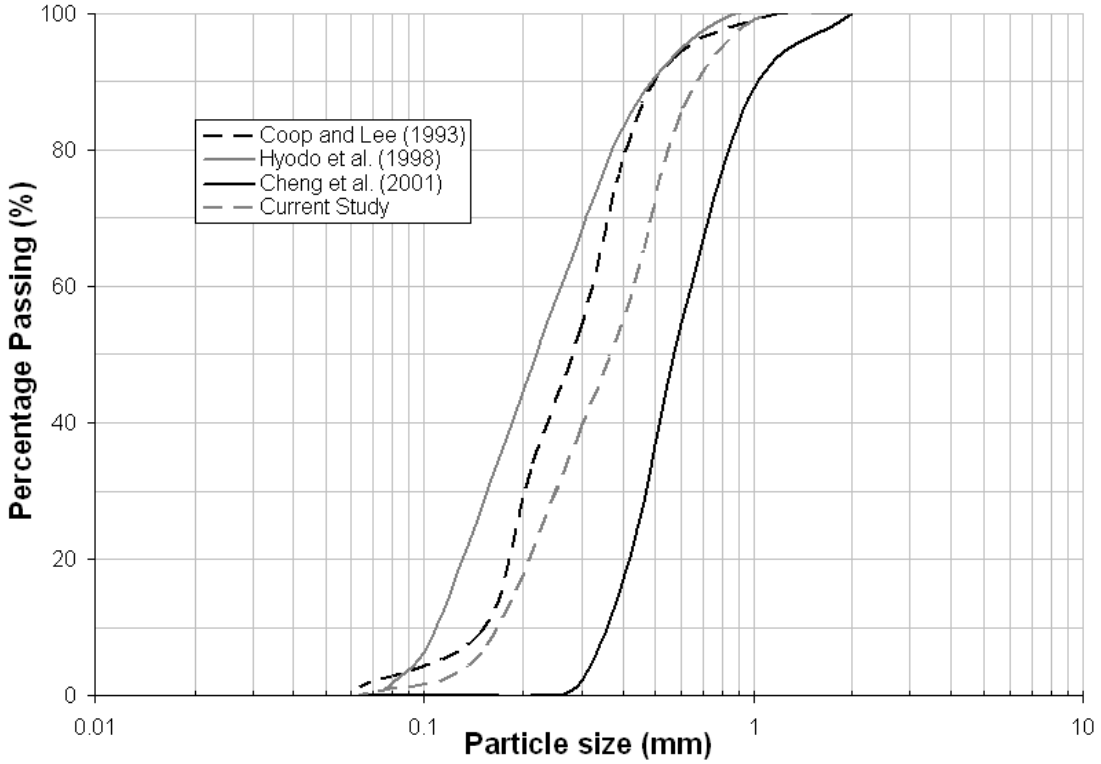

Figure 2 Particle size distribution, comparison of current study with earlier research on Dog's Bay Sand

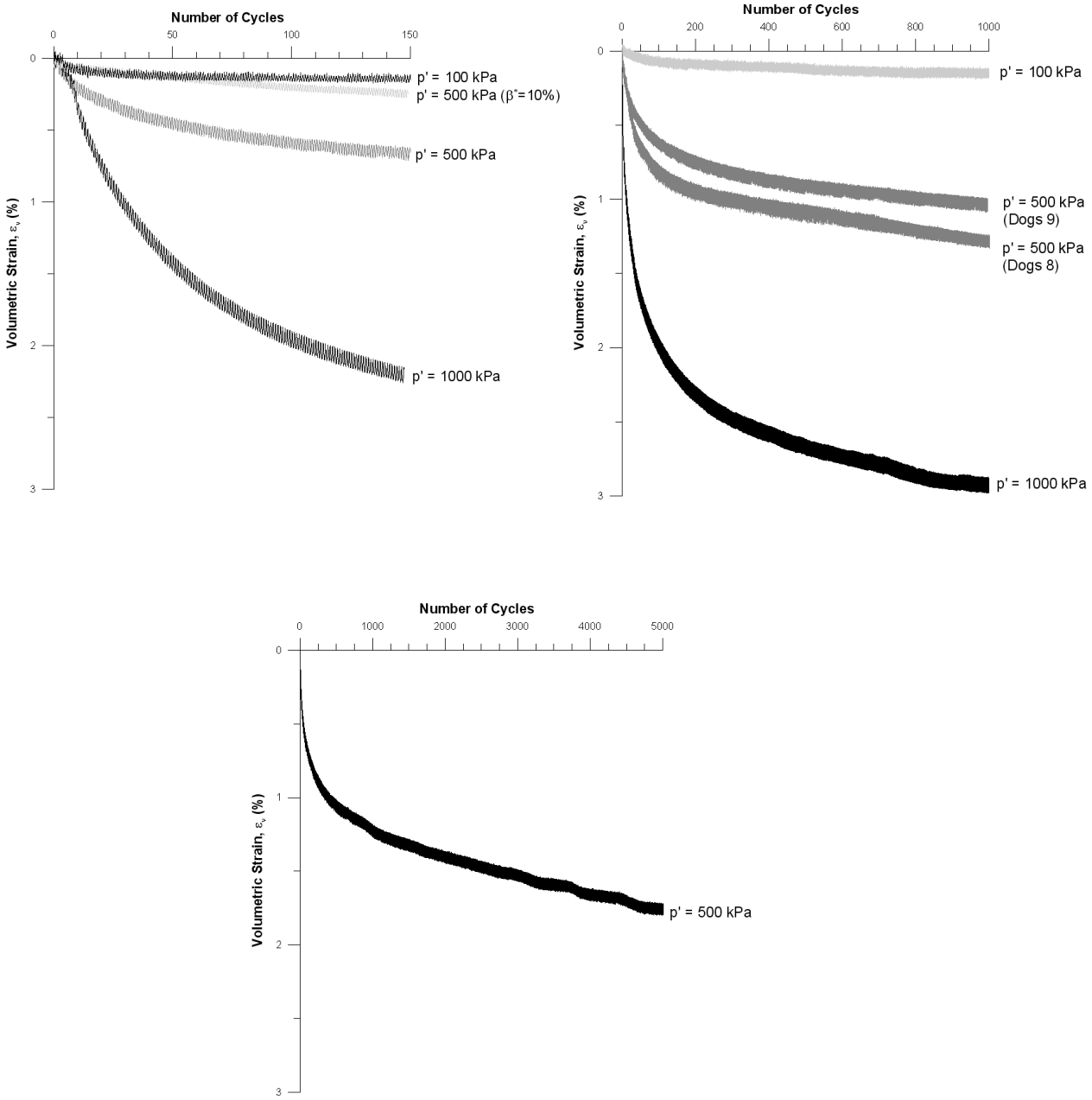

Figure 3 Volumetric strain behaviour during cyclic loading for tests subjected to (a) 150 cycles (b) 1000 cycles (c) 5000 cycles.

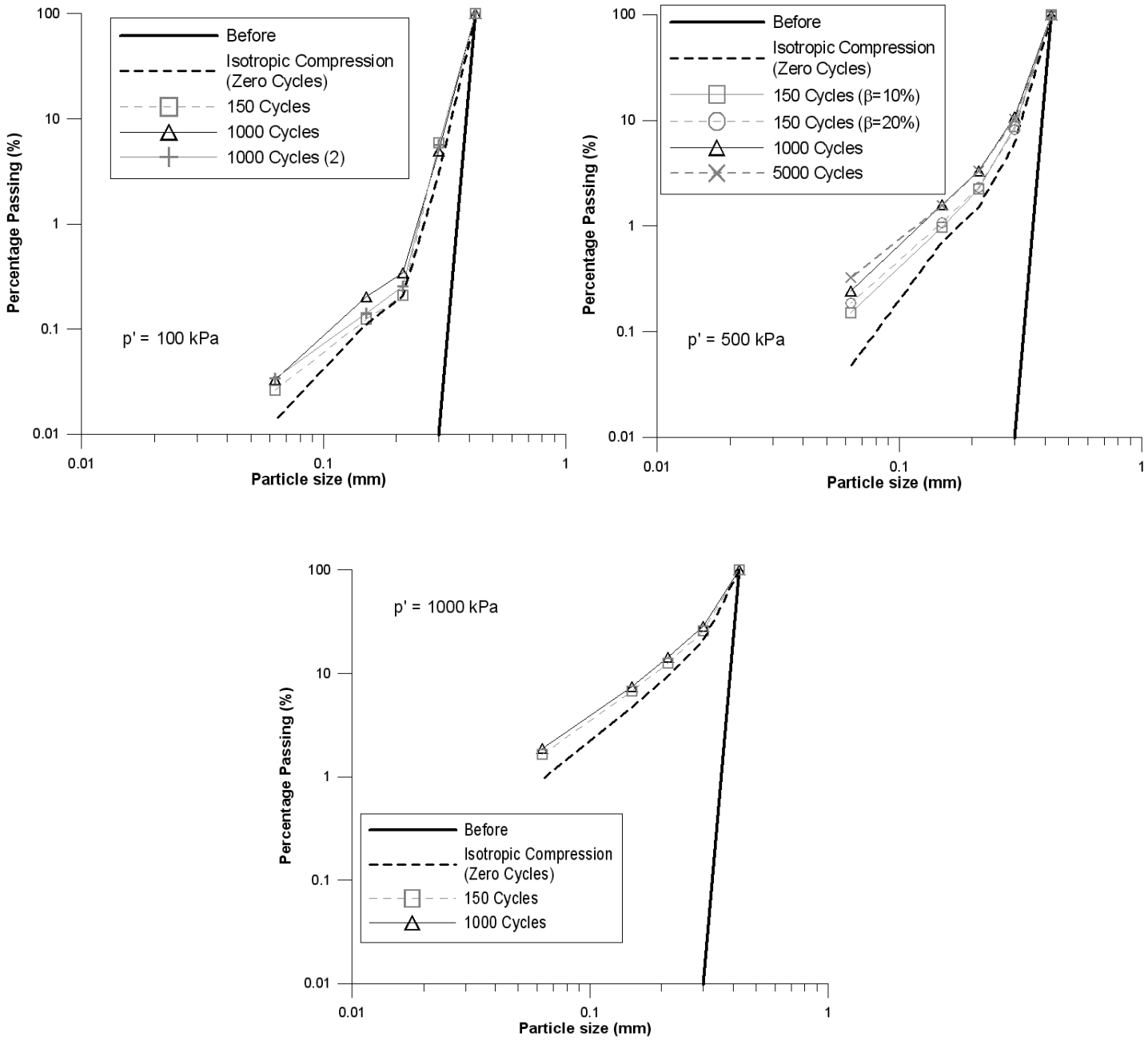

Figure 4 Evolution of particle size distribution for tests at a mean effective stress (p') of (a) 100kPa (b) 500kPa (c) 1000kPa.

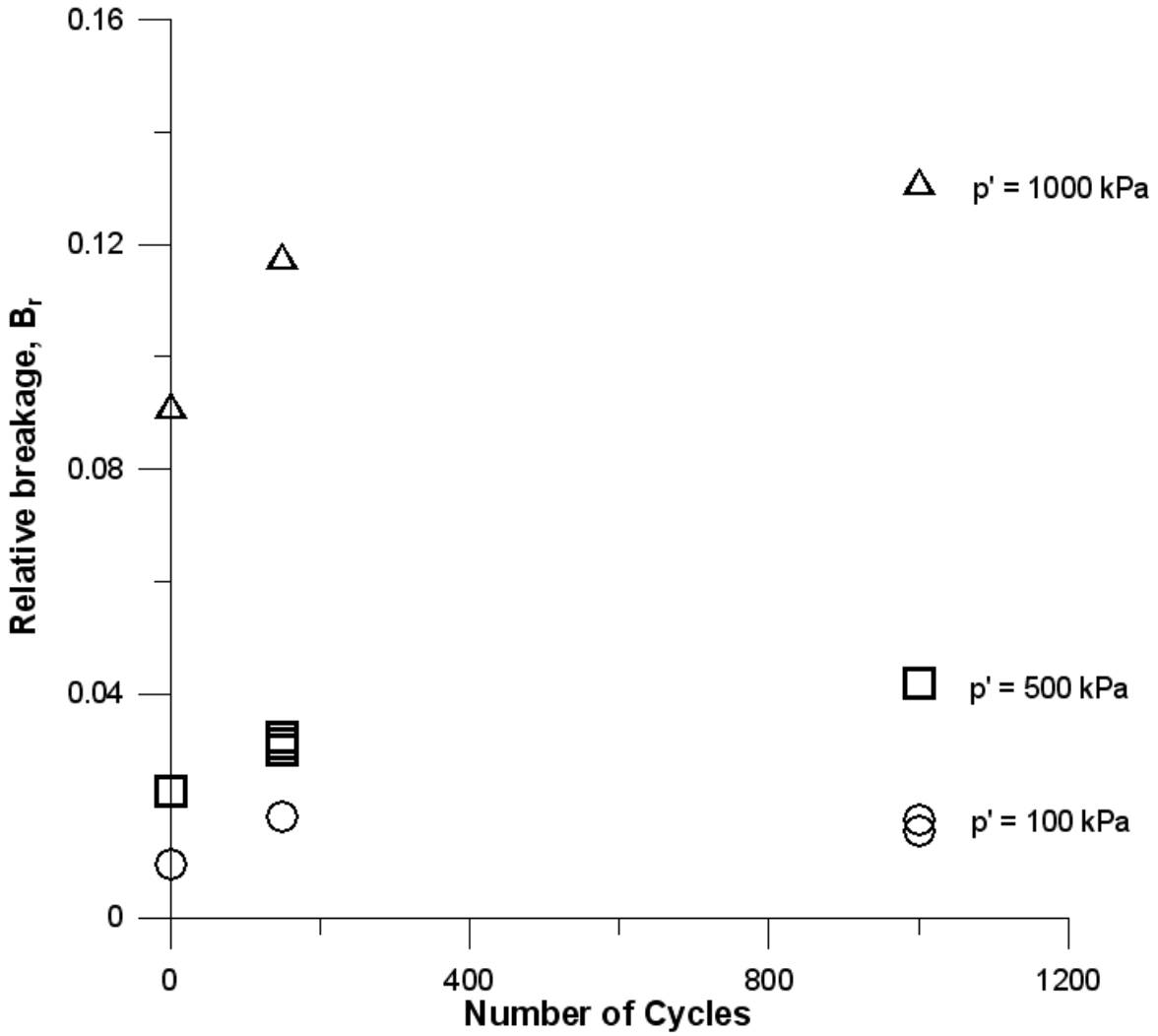

Figure 5 The variation of Hardin's relative breakage with number of cycles.

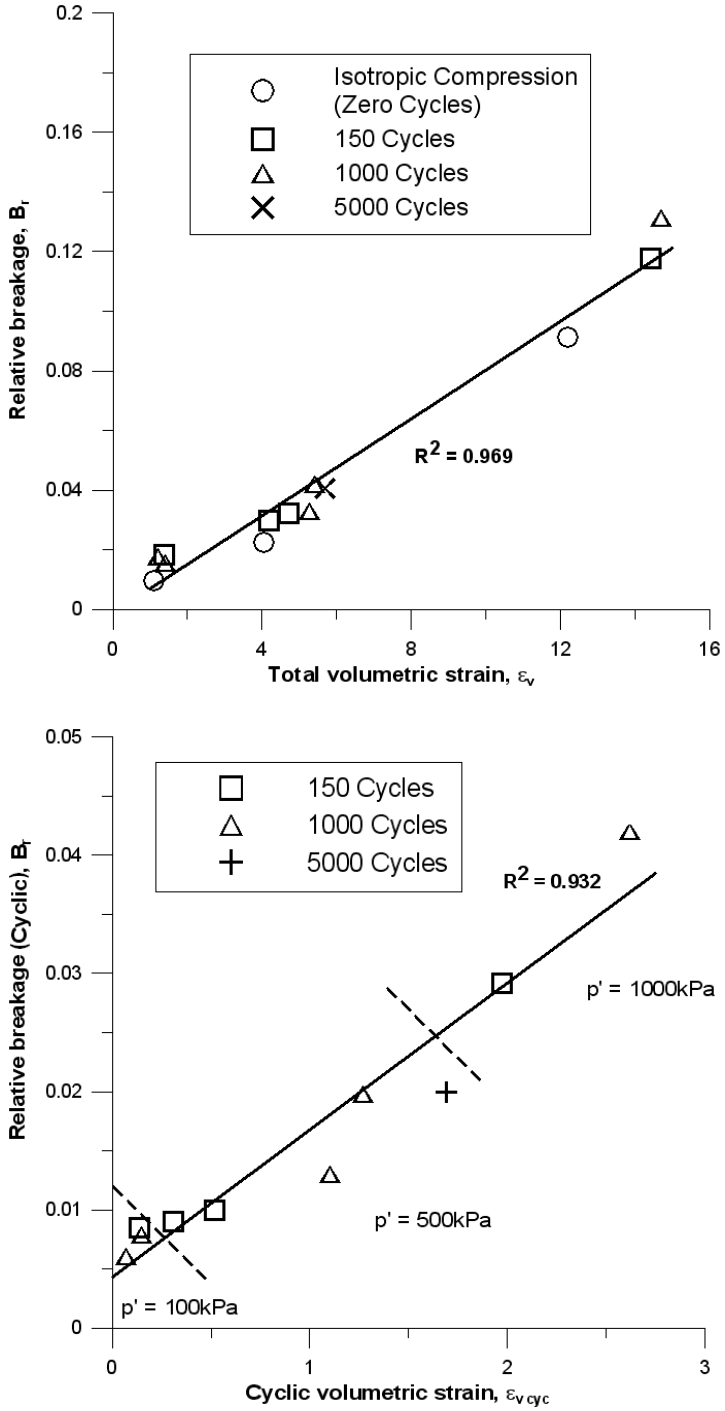

Figure 6 (a) The variation of Hardin's relative breakage with total volumetric strain (isotropic + cycling) (b) The variation of Hardin's relative breakage (cyclic only) with volumetric strain produced during cycling.

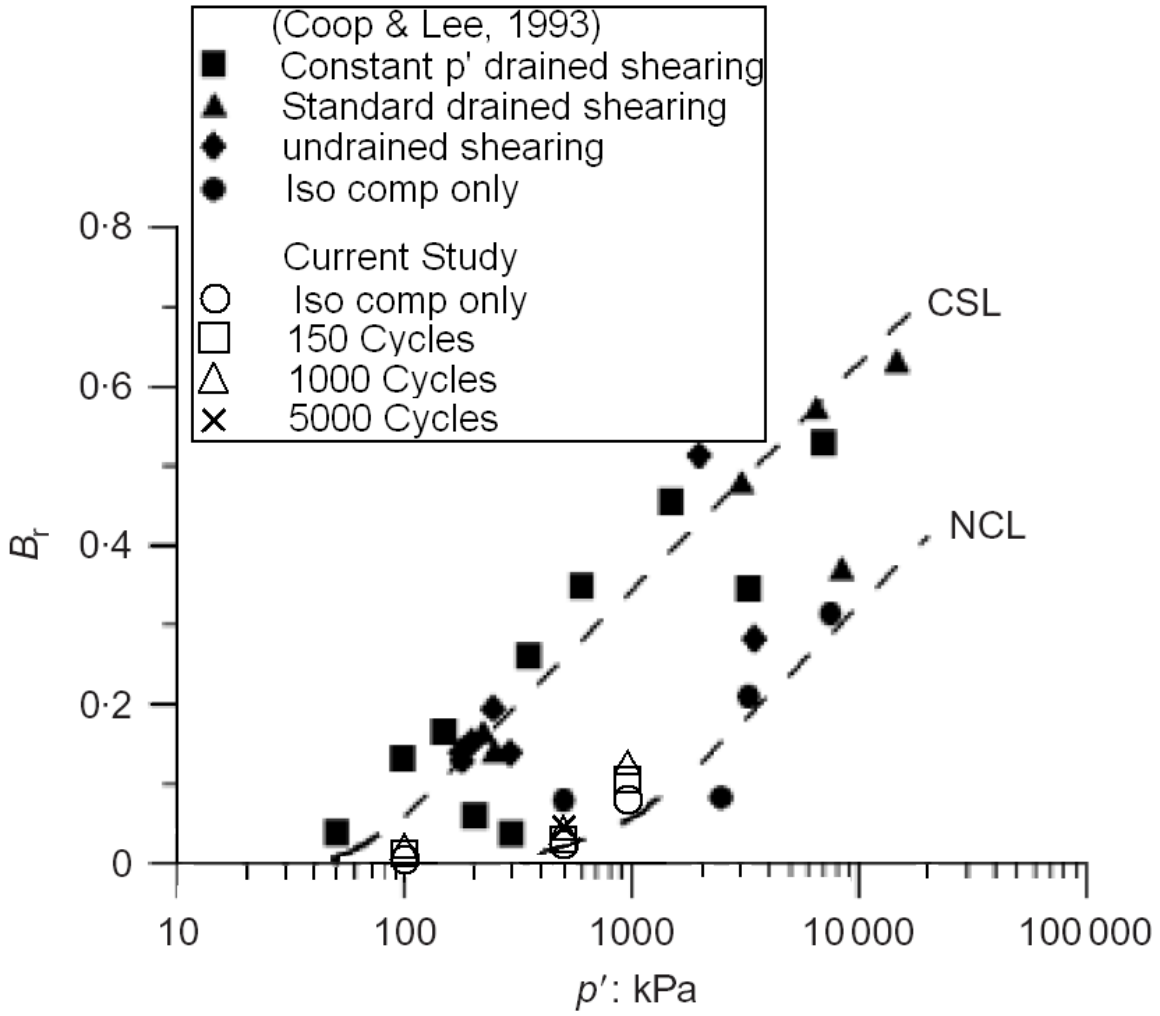

Figure 7 Comparison between particle breakage measured after monotonic loading tests by Coop & Lee, (1993), and tests from this study.